Probing Distance and Electrical Potential within a Protein Pore with Tethered DNA

Stefan Howorka* and Hagan Bayley*†

*Department of Medical Biochemistry and Genetics, The Texas A&M University System Health Science Center, College Station, Texas 77843-1114; and †Department of Chemistry, Texas A&M University, College Station, Texas 77843-3255 USA

ABSTRACT DNA molecules tethered inside a protein pore can be used as a tool to probe distance and electrical potential. The approach and its limitations were tested with α-hemolysin, a pore of known structure. A single oligonucleotide was attached to an engineered cysteine to allow the binding of complementary DNA strands inside the wide internal cavity of the extramembranous domain of the pore. The reversible binding of individual oligonucleotides produced transient current blockades in single channel current recordings. To probe the internal structure of the pore, oligonucleotides with 5′ overhangs of deoxyadenosines and deoxythymidines up to nine bases in length were used. The characteristics of the blockades produced by the oligonucleotides indicated that single-stranded overhangs of increasing length first approach and then thread into the transmembrane β-barrel. The distance from the point at which the DNA was attached and the internal entrance to the barrel is 43 Å, consistent with the lengths of the DNA probes and the signals produced by them. In addition, the tethered DNAs were used to probe the electrical potential within the protein pore. Binding events of oligonucleotides with an overhang of five bases or more, which threaded into the β-barrel, exhibited shorter residence times at higher applied potentials. This finding is consistent with the idea that the main potential drop is across the α-hemolysin transmembrane β-barrel, rather than the entire length of the lumen of the pore. It therefore explains why the kinetics and thermodynamics of formation of short duplexes within the extramembranous cavity of the pore are similar to those measured in solution, and bolsters the idea that a "DNA nanopore" provides a useful means for examining duplex formation at the single molecule level.

INTRODUCTION

The shape of the electrostatic profile within the lumen of transmembrane channels and pores is an important unsettled problem that remains the subject of experimental and theoretical investigation (Hille, 2001). Electrostatics can, for example, make a major contribution to ion selectivity (Imoto et al., 1988; Cheung and Akabas, 1997; Roux and MacKinnon, 1999; Corringer et al., 1999; Wilson et al., 2000). The potential at a point within a pore at a fractional distance "d" from the entrance can be separated into two components, $\psi_M(d)$ and $\psi_S(d)$ (Pascual and Karlin, 1998). In the simplest analysis, $\psi_M(d)$, the electrostatic potential arising from the applied transmembrane potential (ψ_M), is assumed to be a linear function of "d" such that $\psi_M(d) = (1 - d) \cdot \psi_M$ (Fig. 1 *A*). Of course, the actual profile is related to the shape of the lumen. For example, in a channel with a closed gate, almost the entire transmembrane potential drops off across the high resistance constriction. For this reason, the concept of electrical distance (δ) is often used, where $(1 - \delta) \cdot \psi_M$ is the electrostatic potential at "δ" arising from the applied transmembrane potential. When the relationship between $\psi_M(d)$ and "d" is linear, $d = \delta$. In other cases, "δ" increases with "d," but in a more complex manner. The intrinsic electrostatic potential at a point "d," $\psi_S(d)$, arises primarily from permanent charges and dipoles on the protein, together with which factors such as the local dielectric constant and screening by ions within the lumen must be considered (Roux and MacKinnon, 1999).

The large number of adjustable parameters that must be considered make the computation of electrostatic profiles in channels and pores, and the interpretation of related experimental work, a profoundly difficult task. Nevertheless, progress has been made both in computation (Adcock et al., 1998; Roux and MacKinnon, 1999) and measurement (Stauffer and Karlin, 1994; Chiamvimonvat et al., 1996; Cheung and Akabas, 1997; Pascual and Karlin, 1998; Wilson et al., 2000). In the case of narrow ligand- or voltage-gated channels the contribution of $\psi_S(\delta)$ to the potential at a point in the lumen is comparable with or greater than the contribution of $(1 - \delta) \cdot \psi_M$. However, in pores of large diameter, particularly at high salt concentrations, $(1 - \delta) \cdot \psi_M$ is likely to dominate. Here, we study the dynamics of a DNA probe tethered within the staphylococcal α-hemolysin (αHL) pore. Our results are consistent with the notion that the applied transmembrane potential drops off slowly in the internal *cis* cavity of the pore and more rapidly in the transmembrane β-barrel (Fig. 1 *B*).

The mushroom-shaped heptameric transmembrane pore formed by αHL, a 293-residue bacterial toxin, has interesting internal dimensions (Song et al., 1996). The mushroom cap, which is found on the *cis* side of the lipid bilayer (Fig. 1 *B*), contains a large cavity, which measures ~46 Å in

Submitted November 21, 2001, and accepted for publication August 5, 2002.

Address reprint requests to Hagan Bayley, Ph.D., Department of Medical Biochemistry and Genetics, The Texas A&M University System Health Science Center, 440 Reynolds Medical Building, College Station, TX 77843-1114. Tel.: 979-845-7047; Fax: 979-862-2416; E-mail: bayley@tamu.edu.

Dr. Howorka's present address is Upper Austrian Research, Scharitzerstrasse 6–8, A-4020, Linz, Austria.

0006-3495/02/12/3202/09 $2.00

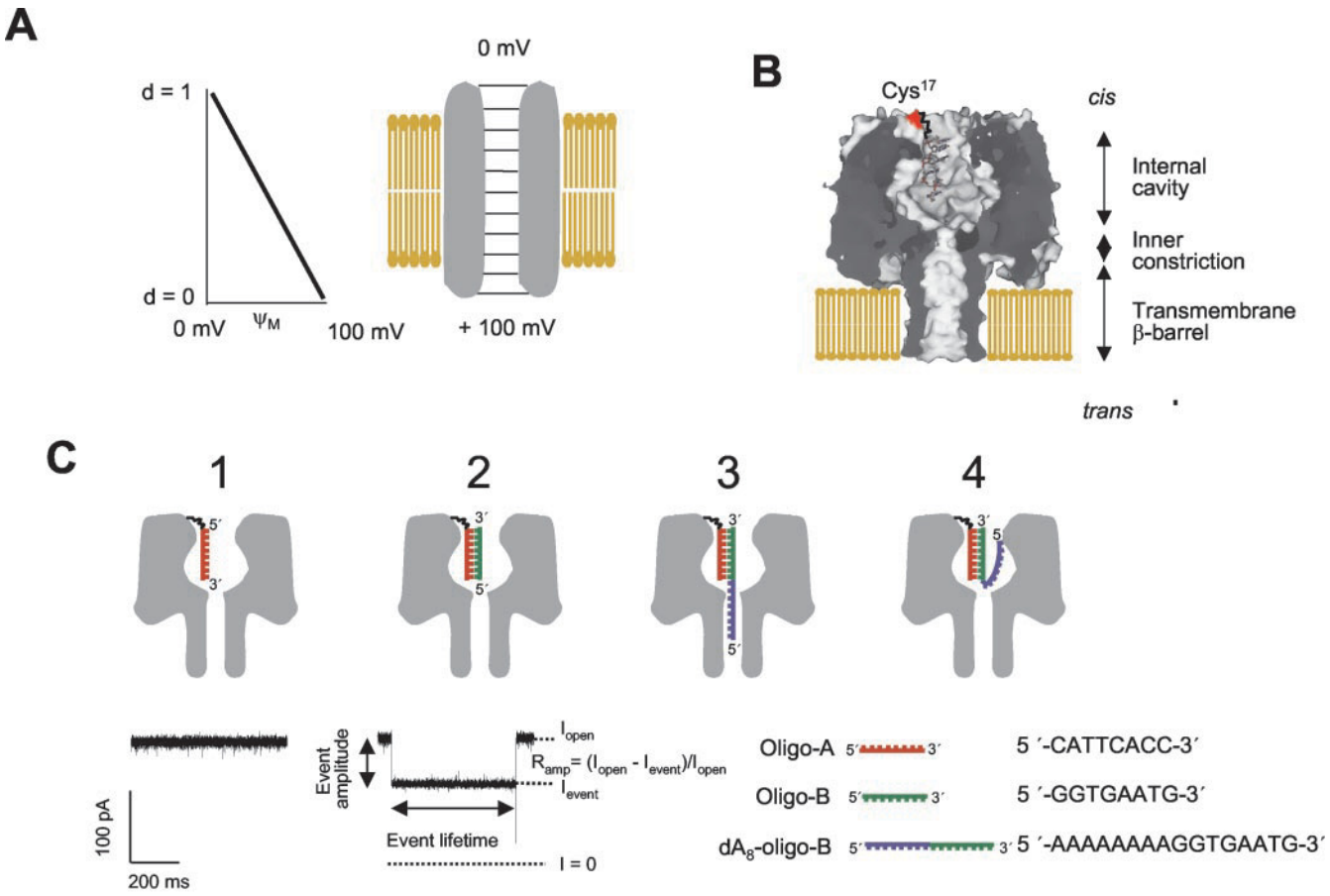

FIGURE 1 Binding of individual complementary oligonucleotides inside the αHL pore. (*A*) Section through an idealized pore showing lines of equipotential. (*B*) Cross-section through the heteroheptameric αHL pore $H_6$17C-oligo-A_1 containing one subunit modified with DNA and six unmodified subunits. The 5′-end of the oligonucleotide is attached via a hexamethylene linker and a disulfide bond to Cys-17. (*C*) Schematic drawings of the protein pore $H_6$17C-oligo-A_1 (panel *C*-1) with bound oligonucleotide oligo-B (panel *C*-2) and dA_8-oligo-B (panels *C*-3 and *C*-4). Panel *C*-3 represents state B of a type 2 event and panel *C*-4 a type 1 event (see the text for further explanation). The sequence of oligo-B (5′-GGTGAATG-3′) is complementary to the sequence of the tethered oligo-A (5′-CATTCACC-3′). Transient binding of oligo-B to oligo-A produces reversible current blockades with a characteristic amplitude reduction, R_{amp} (*C*-2, bottom panel). The current traces were filtered at 10 kHz and sampled at 50 kHz.

internal diameter and is entirely located within the extramembranous domain. In the transmembrane domain, the pore lumen narrows to form a 14-stranded β-barrel with an average internal diameter of ~20 Å. The two domains are separated by a constriction of diameter ~14 Å (Fig. 1 *B*). In previous studies on other proteins, detailed electrostatic profiles have been obtained by mutating the target protein so that reactive cysteine residues are located at strategic positions within the lumen. The rate of reaction with charged reagents is then measured for each mutant (Chiamvimonvat et al., 1996; Pascual and Karlin, 1998) and a profile can be obtained in terms of the electrical distance δ. Here, we take on a simpler task and ask how the applied potential falls off in the extramembranous domain of the αHL pore as compared with the transmembrane barrel. A DNA oligonucleotide is tethered at a fixed position near the *cis* entrance of the pore (Fig. 1 *B*). Probe nucleotides of different lengths can then be attached by duplex formation and used to sense the potential at defined depths within the lumen. While the approach is limited by the large dimensions of the DNA probe, in the case of a pore such as αHL, it does provide useful information.

MATERIALS AND METHODS

Oligonucleotides

Unless otherwise stated, DNA oligonucleotides were purchased from Integrated DNA Technologies (Coralville, IA). The purity of the oligonucleotides was checked by non-denaturing polyacrylamide gel electrophoresis (Chory and Pollard, 1999). Instead of TBE buffer, TAE (40 mM Tris acetate, 2 mM EDTA, pH 8.0) was used to prepare the gel and the running buffer. After electrophoresis, the gels were stained for 2 min in a 0.2% aqueous solution of 1-ethyl-2-[3-(1-ethylnaphtho[1,2-d]thiazolin-2-ylidene)-2-methylpropenyl]naphtho[1,2-d]thiazolium bromide (Stains-all; Sigma, St. Louis, MO, E-9379) containing 50% formamide, and destained in water for 20 min. Destained gels were scanned and analyzed using the software Scion Image. DNA oligonucleotides of up to 10 nucleotides

contained <2% of truncated products, and oligonucleotides of between 10 and 17 nucleotides <6%.

αHL heptamers modified with single DNA oligonucleotides

αHL heptamers modified with single DNA oligonucleotides were generated as described (Howorka et al., 2001a,b). Briefly, 5′-thiol-modified DNA oligonucleotides with a hexamethylene linker (Research Genetics, Huntsville, AL) were activated with 2,2′-dithiodipyridine to yield 5′-S-thiopyridyl oligonucleotides (Corey et al., 1995). The activated oligonucleotides were coupled to the in vitro expressed (Cheley et al., 1999) mutant, αHL-17C-D4 (Howorka et al., 2001a,b). Modified αHL-17C-D4 and unmodified wild-type monomers (H) were then coassembled on erythrocyte membranes and the resultant heptamers were purified by SDS-polyacrylamide gel electrophoresis (Howorka et al., 2000). Heptamers with different subunit compositions migrated in separate bands due to a gel shift caused by the C-terminal polypeptide extension of four aspartates (D4) (Howorka et al., 2001b). Heptameric $H_6$17C-oligo$_1$ was extracted from gel slices as described (Howorka et al., 2000).

Bilayer recordings

Electrical recordings were carried out with a planar lipid bilayer apparatus at 22 ± 1.5°C (Montal and Mueller, 1972; Hanke and Schlue, 1993; Braha et al., 1997). A bilayer of 1,2-diphytanoyl-*sn*-glycero-3-phosphocholine (DPPC) was formed on a 100-μm orifice in a Teflon septum (25 μm thick; Goodfellow Corporation, Malvern, PA), which separated the two compartments of the apparatus. The chambers contained 1.3 ml of 2 M KCl, 12 mM $MgCl_2$, 5 mM Tris-HCl, pH 7.4. Bilayers were formed by first treating the surface around the orifice with a solution of hexadecane in n-pentane (10 mg/ml). Then, DPPC dissolved in n-pentane (10 mg/ml) was allowed to spread on top of the electrolyte in both compartments. After the solvent had evaporated, a bilayer was formed by lowering and raising the electrolyte level once with respect to the orifice. Heptameric protein was then added to the *cis* compartment to a final concentration of 0.01 to 0.1 ng/ml, and the electrolyte was stirred until a channel inserted. Recordings were performed at an applied potential of +100 mV, unless otherwise stated, with the *cis* chamber grounded. In general, the currents were low-pass filtered with a 4-pole Bessel filter at 10 kHz, sampled at 50 kHz by computer with a Digidata 1200 A/D converter (Axon Instruments, Union City, CA) and analyzed as described (Movileanu et al., 2000). For the analysis of the lifetimes of the binding events and their dependence on the length of the single-stranded extension (Fig. 4), signals were filtered at 1 kHz and sampled at 5 kHz. In general, current traces displayed in the figures were filtered at 10 kHz and sampled at 50 kHz. Current traces in Fig. 5 *A* were filtered at 1 kHz and sampled at 5 kHz.

RESULTS

The current signatures of covalently attached DNA duplexes depend on the lengths of their single-stranded extensions

An αHL heptamer, $H_6$17C-oligo-A_1, with an oligonucleotide, oligo-A, attached covalently at position 17 of the single derivatized subunit (Fig. 1 *B*) was prepared by a procedure devised previously (Howorka et al., 2001b). The attachment of the single-stranded oligonucleotide decreases the conductance of the αHL pore by ~7% in 2 M KCl, the salt concentration used in this work, and by ~17% in 1 M KCl and ~4% in 3.5 M KCl. Oligo-A served to anchor a series of oligonucleotides based on oligo-B near the *cis* mouth of the pore. Oligo-B is fully complementary to oligo-A, and the other nucleotides in the series consisted of oligo-B with 5′-oligo dA extensions, for example, dA_8-oligo-B (Fig. 1 *C*). Oligo-B presented from the *cis* chamber binds to the immobilized oligo-A to produce a transient current blockade at an applied potential of +100 mV (Fig. 1 *C*-2 and Fig. 2 *A*-0) (Howorka et al., 2001a,b). The block was characterized by an amplitude reduction (R_{amp}) of 0.32, where R_{amp} is defined as the ratio of the event amplitude to the mean current through the modified pore before the oligonucleotide binding event (Fig. 1 *C*-2 and Fig. 2 *A*-0).

The remaining oligonucleotides in the series, dA_1-oligo-B through dA_8-oligo-B, also bound, each giving a characteristic R_{amp} value and current signature (Fig. 2 *A*, panels 1 through 8-1). The R_{amp} value for dA_1-oligo-B was slightly increased over oligo-B, with no extension. For dA_N-oligo-B with $N \geq 2$, two types of events were observed. Type 1 events comprised ~15% of the total number of events and had an R_{amp} value that was independent of the length of the extension and similar to R_{amp} for oligo-B, the oligonucleotide without an extension (Fig. 2 *A*, panel 8-2; Fig. 2 *B*, *open circles*). R_{amp} of the type 2 events (~85% of the total) increased with the length of the extension (Fig. 2 *A*, panels 2 through 8-1; Fig. 2 *B*, *black squares*). In the case of dA_2-oligo-B, the type 2 events exhibited slight excess noise when compared with the oligo-B and dA_1-oligo-B events. In the case of dA_3-oligo-B, the excess noise was readily apparent. For $N \geq 4$, the signatures of the events indicate the presence of two current levels and transitions between them: state A (higher conductance), state B (lower conductance). The midpoint of the transition to the lower conductance state was at $N = 5$, at an applied potential of +100 mV (Fig. 2, *B* and *C*).

The events arising from the shorter extensions, oligo-B and dA_1-oligo-B through dA_3-oligo-B (Fig. 2 *A*, panels 0 through 3), exhibit an "exit spike." It is likely that the spike arises as the oligonucleotide dissociates to the *trans* side in the positive applied potential, and in doing so passes through the inner constriction of the pore. A similar signal was seen by Vercoutere and colleagues when DNA hairpins unfolded at the *cis* entrance and passed through the αHL pore (Vercoutere et al., 2001).

We also studied the binding of oligo-B with 5′-dT extensions. The first oligonucleotide in the series, dT_1-oligo-B, bound to immobilized oligo-A (Fig. 3 *A*-1) with an R_{amp} value of 0.36 that was slightly higher than R_{amp} for the oligonucleotide without the extension, oligo-B. The other oligonucleotides in the series, dT_2-oligo-B through dT_9-oligo-B, also bound to oligo-A, each giving a characteristic R_{amp} and current signature (Fig. 3 *A*, panels 2–9). As noted for the 5′-dA extensions, type 1 events of the dT_N-oligo-B series had an amplitude reduction that was independent of the length of the extension (Fig. 3 *B*, *open circles*). Type 2 events comprised ~90% of the total number of events, with the exception of dT_9-oligo-B (66% of the events). In the case of dT_2-oligo-B,

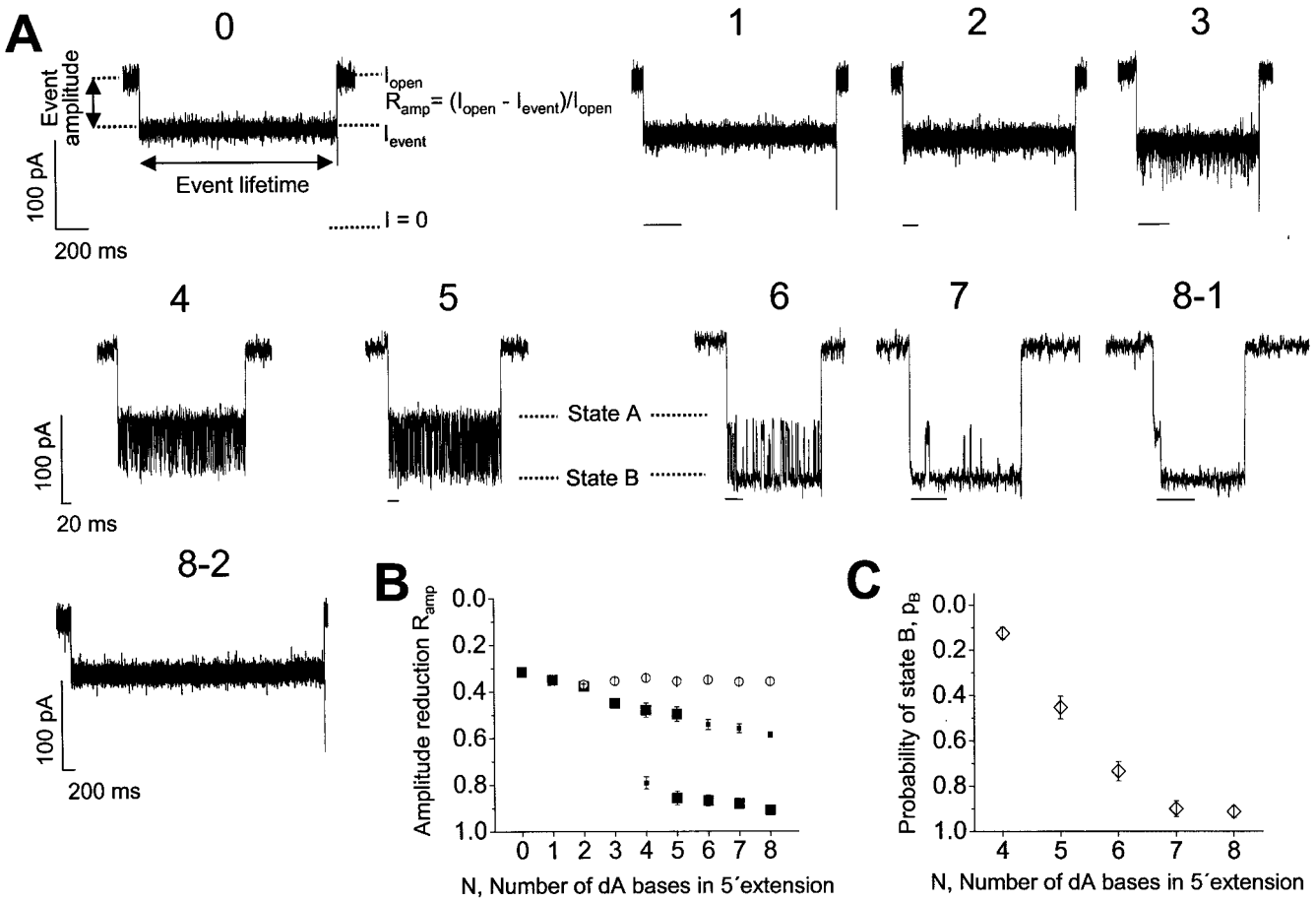

FIGURE 2 Probing the structure of the αHL pore with tethered oligonucleotides with dA extensions of various lengths. (*A*) Segments of representative single channel current traces of the αHL pore $H_6$17C-oligo-A_1 displaying individual binding events of oligonucleotides oligo-B (0), dA_1-oligo-B (1), dA_2-oligo-B (2), dA_3-oligo-B (3), dA_4-oligo-B (4), dA_5-oligo-B (5), dA_6-oligo-B (6), dA_7-oligo-B (7), and dA_8-oligo-B (8-1 and 8-2). (*B*) Dependence of the event amplitudes on the length of the dA extension. *Filled squares:* R_{amp} values for the type 2 events (at least 85% of all binding events). *Open circles:* R_{amp} values for the type 1 events (≤15% of all events). Event amplitudes were obtained by current histogram analysis. The amplitudes at the Gaussian-shaped peak of maximum occurrence in the histograms were normalized to the current of the unblocked $H_6$17C-oligo-A_1 pore to yield the amplitude reduction, R_{amp}. For the type 2 events of dA_4-oligo-B through dA_8-oligo-B, two states (A and B) are seen; the dominant state is indicated by the larger symbol. The points represent the means of five different recordings ($n = 5$); the vertical bars indicate the standard deviation (SD). (*C*) The probability of state B (p_B) during type 2 binding events is plotted versus the length of the dA extension ($n = 3$, ±SD). p_B was obtained after deriving the occupancies of states A and B from all-points histograms; there was one peak for state A and one for state B (if present). The current traces were filtered at 10 kHz and sampled at 50 kHz.

the type 2 events exhibited slight excess noise when compared with the oligo-B and dT_1-oligo-B events. In the case of dT_3-oligo-B, the excess noise was readily apparent. For dT_4-oligo-B and longer oligonucleotides, two current levels were again observed, although the occupancy of state B was low for dT_4-oligo-B. The midpoint of the transition to the lower conductance state B was between $N = 6$ and $N = 7$, at an applied potential of +100 mV (Fig. 3, *B* and *C*).

The lifetimes of the DNA duplexes are dependent on the lengths of the single-stranded extensions

The lifetimes of the binding events were determined for oligo-B, dA_1-oligo-B through dA_8-oligo-B, and dT_1-oligo-B through dT_9-oligo-B. The average duration of the type 1 events did not vary greatly with the length of the extension. For dA_2-oligo-B through dA_8-oligo-B the mean duration was 1090 ms, and for dT_2-oligo-B through dT_9-oligo-B, 840 ms. By contrast, the lifetimes of the type 2 binding events for dA_N-oligo-B oligonucleotides were dependent on the length of the extension. The lifetimes were obtained from dwell-time histograms, which could be fitted with single exponentials (data not shown). As seen in a plot of lifetime versus the number of bases, *N*, in the extension (Fig. 4 *A*), the longest lifetime was observed for $N = 1$. For $N \geq 2$, the event duration decreased with increasing length up to $N = 7$. The lifetime for $N = 8$ was slightly higher than $N = 7$. Similar behavior was observed for the type 2 events

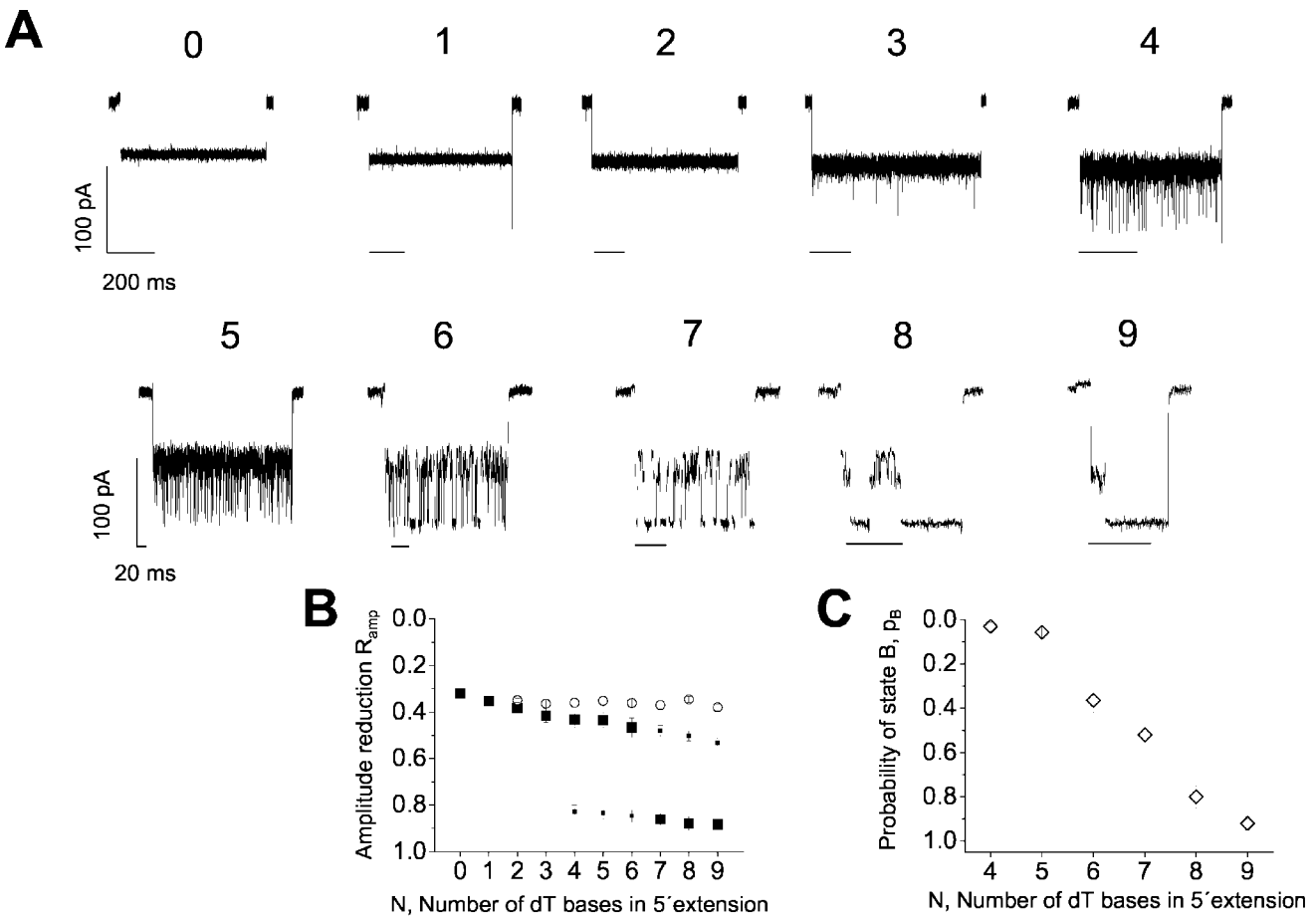

FIGURE 3 Probing the structure of the αHL pore with tethered oligonucleotides with dT extensions of various lengths. (*A*) Segments of representative single channel current traces of the αHL pore $H_6$17C-oligo-A_1 displaying individual binding events of oligonucleotides oligo-B (0) and oligonucleotides dT_1-oligo-B (1) through dT_9-oligo-B (9). (*B*) Dependence of R_{amp} on the length of the dT extension. *Filled squares:* type 2 events (at least 90% of all binding events, except for dT_9-oligo-B, where the percentage of type 2 events was 66%). For dT_4-oligo-B through dT_9-oligo-B, two states (A and B) are seen; the dominant state is indicated by the larger symbol. *Open circles:* type 1 events (≤10% of all events, except for dT_9-oligo-B). The points represent the means of three different recordings; the vertical bars indicate the standard deviation (SD). The event amplitudes were obtained from all-points histograms. For oligonucleotides with dT extensions with $4 \leq N \leq 8$, two peaks were observed for state A (traces 6–8), which were about equally populated. In these cases, the difference between the currents at the two maxima ranged from 16 pA (dT_6 extension) to 22 pA (dT_8 extension) and the arithmetic mean was used to determine R_{amp}. (*C*) The probability of state B (p_B) during type 2 binding events, obtained from all-points histograms, is plotted versus the length of the dT extension ($n = 3$, ±SD). For oligonucleotides with dT extensions with $4 \leq N \leq 8$, the two substates of state A were combined to give one probability for state A. The current traces were filtered at 10 kHz and sampled at 50 kHz.

associated with oligonucleotides with 5′-dT extensions (Fig. 4 *B*). Again, the lifetime increased for $N = 1$ over $N = 0$, and dropped from this maximum for extensions of $N \geq 2$.

The current signatures and lifetimes of the DNA duplexes are voltage-dependent

We studied the influence of the applied potential on the amplitude reduction and the fine structure of dA_5-oligo-B binding events (Fig. 5 *A*). At +70 mV, the amplitude reduction, R_{amp}, derived from the major conductance level was 0.57. Higher potentials led to a shift in the amplitude reduction: +100 mV, $R_{amp} = 0.56$ and 0.77; +130 mV, $R_{amp} = 0.79$; and +160 mV, $R_{amp} = 0.82$. Once more, the signatures of the events suggest two current levels. In this case, the occupancy of the lowest conducting state, state B, increases with voltage rather than chain length: +70 mV, $p_B = 0.12$; +100 mV, $p_B = 0.51$; +130 mV, $p_B = 0.75$; and +160 mV, $p_B = 0.92$.

Next, the influence of the applied potential on the lifetimes of the oligonucleotide binding events was investigated. The voltage-dependence of the lifetime was determined for two extreme cases: oligonucleotides with the longest extensions, dA_8-oligo-B and dT_9-oligo-B, and oligonucleotides without extensions. The durations of dA_8-oligo-B and dT_9-oligo-B binding events were determined by fitting single exponentials to lifetime histograms (not shown) and were found to decrease with increasing poten-

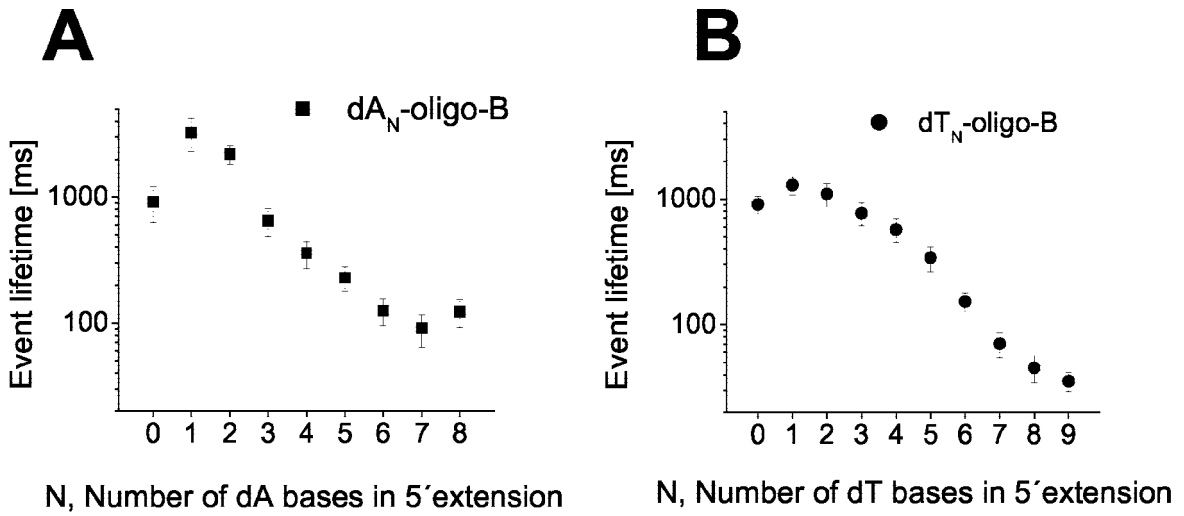

FIGURE 4 The lifetimes of type 2 oligonucleotide binding events are dependent on the length of the extension in oligo-B. (*A*) dA extensions; (*B*) dT extensions. The plotted values are the means (±SD) of single-exponential fits to three independent recordings, each containing between 700 and 1500 events.

tial (Fig. 5 *B*). The event lifetimes (τ) for dA_8-oligo-B (Fig. 5 *B*, *filled diamonds*) exhibit a subexponential voltage dependence indicating that τ tends toward a constant value at high potentials. By comparison, the lifetimes for dT_9-oligo-B events (Fig. 5 *B*, *open squares*) were shorter, at a given voltage, than those for dA_8-oligo-B, but also exhibited a subexponential dependence on applied potential.

In contrast to the negative voltage dependencies of the lifetimes of duplexes formed by oligo-B with dA_8 or dT_9 extensions, the mean event durations for unextended oligo-B increased linearly with voltage (Fig. 5 *C*) with a slope of 10 ms mV^{-1}. A positive voltage dependence of the lifetimes was also observed for another oligonucleotide without an extension. Oligo-D, an 8-mer like oligo-B but with a different sequence (5′-TACGTGGA-3′), also forms a duplex with a complementary oligonucleotide tethered within the pore (Howorka et al., 2001b). The lifetimes for oligo-D show a linear voltage dependence with a slope of 3.5 ms mV^{-1}.

DISCUSSION

In the engineered αHL heptamer, $H_6$17C-oligo-A_1, the attached oligonucleotide, the 8-mer oligo-A, is capable of hybridizing to a complementary oligonucleotide, oligo-B, as shown previously (Howorka et al., 2001a,b) and here (Fig. 1 *C*-2). The binding events were manifested as a sudden jump to a lower conductance state. A spike of even lower conductance appeared upon dissociation as the detached oligo-B made its way through the constriction in the lumen of the pore (Fig. 1 *B*) (Vercoutere et al., 2001; Howorka et al., 2001a). Interestingly, the covalent attachment of a single-stranded oligonucleotide decreases the conductance of the αHL pore by ~7%, while the formation of a duplex with the same attached DNA strand gives a much larger reduction in conductance of ~38% compared to the unmodified pore. The reason for this is not certain, but perhaps it is related to the greater stiffness of double-stranded DNA compared with single-stranded DNA.

When the hybridizing oligonucleotide was extended by one dA base, the general appearance of the binding events was unchanged. However, further increases in the length of the extension first produced events that were noisy, indicating that the oligonucleotide approaches the internal constriction (dA_2-oligo-B to dA_3-oligo-B), and then a signal characteristic of two states (dA_4-oligo-B to dA_8-oligo-B), indicating that the oligonucleotide enters the transmembrane β-barrel. We assign the higher conductance state A to a conformation in which dA_N-oligo-B is entirely in the cavity, and the lower conductance state B to a conformation in which the 5′-end of dA_N-oligo-B extends through the inner constriction into the barrel (Fig. 1 *C*-3).

This behavior is similar to that of the highly flexible polymer poly(ethylene glycol), PEG, when it is tethered by one end within the cavity (Howorka et al., 2000; Movileanu et al., 2000). The presence of PEG in the cavity leads to a relatively small conductance decrease, but the occasional threading of the free PEG end into the β-barrel is accompanied by a larger drop in conductance. For the DNA-modified pore, the duplex in state A is thought to be localized in the cavity and exhibits a current blockade that increases slightly with the length of the extension (Fig. 2 *B*). The extent of block in state B is higher than in state A, and also increases with the length of the extension for dA_4 and higher. The amplitude of state B approximates the amplitude of the exit spike, which is clearly visible in the traces for dA_N-oligo-B with $N \leq 3$, but not for $N \geq 4$ (Fig. 2 *B*). This finding supports the idea that state B arises from the penetration of the oligonucleotide extension into the β-barrel.

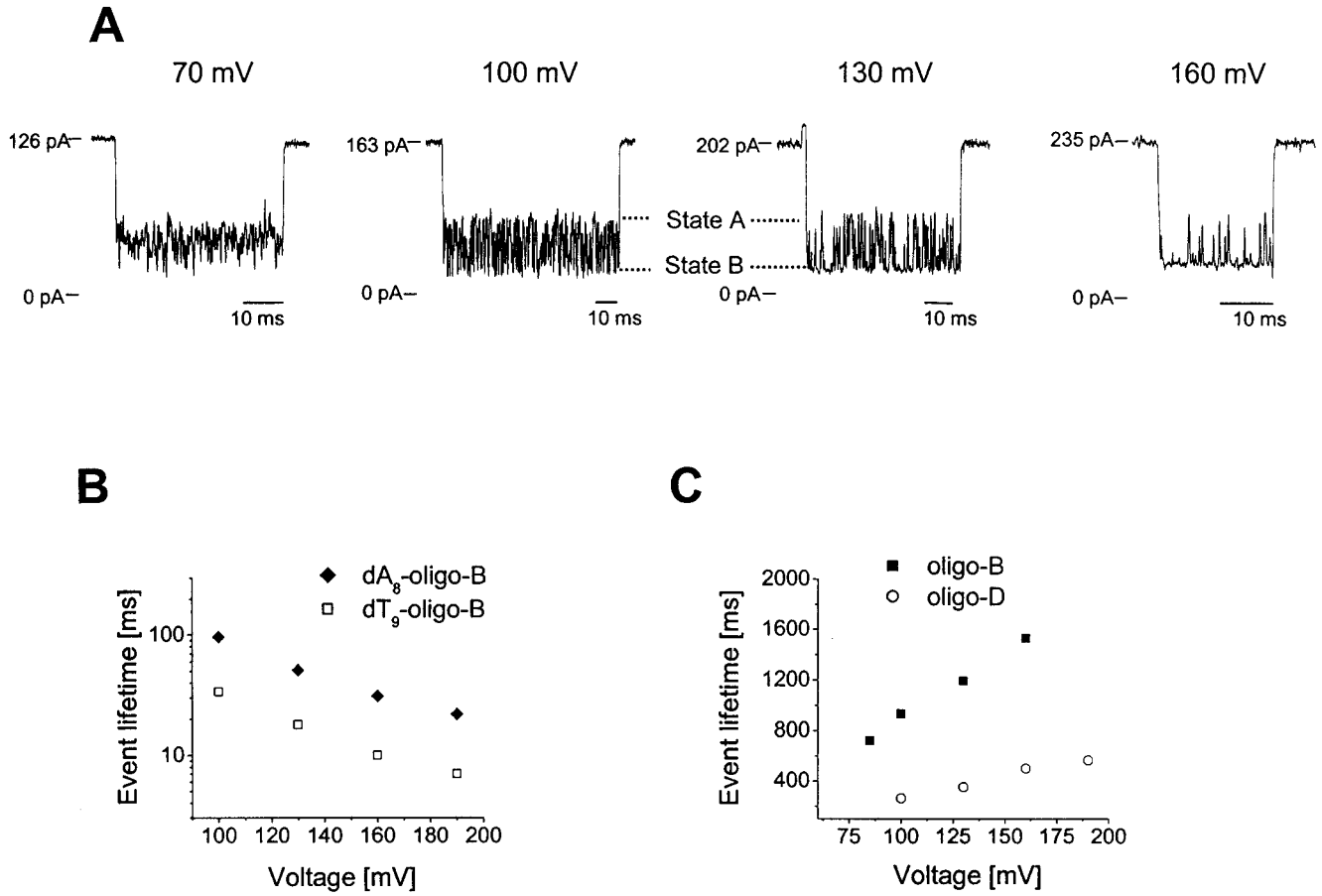

FIGURE 5 Voltage-dependence of type 2 oligonucleotide binding events. (*A*) An increase in the applied potential changes the event amplitude and the fine structure of dA_5-oligo-B binding events. Representative segments of current traces are shown at +70 mV, +100 mV, +130 mV, and +160 mV. The current traces were filtered at 1 kHz and sampled at 5 kHz. (*B*) Voltage-dependence of binding events for dA_8-oligo-B and dT_9-oligo-B. (*C*) Voltage-dependence of oligo-B and oligo-D binding events. Oligo-D, an 8-mer like oligo-B but with a different sequence (5′-TACGTGGA-3′) forms a duplex with a complementary oligonucleotide oligo-C tethered within the pore. Typical experiments are shown in *B* and *C*. The experiments were repeated and gave the same voltage-dependencies.

In many cases, the binding events are initiated by a transient increase in conductance of unknown origin, which was more readily apparent with a lower frequency filter cutoff (but see Fig. 2 *A*, traces 4, 5, and 8−1; and Fig. 3 *A*, traces 6 and 8). As noted in Results, a small fraction of events (type 1, Fig. 1 *C*-4) were featureless (e.g., Fig. 2 *A*, panel 8−2) and most likely arise from another state, distinct from state A, in which the duplex is confined to the cavity. This interpretation is supported by the finding that the duration of type 1 events is voltage-independent. Therefore, in this case, it is unlikely that the extension penetrates into the β-barrel, where it would "feel" the transmembrane potential (see below). Transitions between the type 1 and type 2 states were rare (data not shown).

As expected, the occupancy of state B in the type 2 events for dA_N-oligo-B with $N \geq 4$ increases with the length of the 5′-extension, most likely because, in going from state A to state B, the movement ($z \cdot \Delta\delta$) of the negatively charged backbone of the DNA strand in the transmembrane potential of +100 mV increases with length. The data, however, do not support the notion that dA_3 extensions penetrate into the β-barrel to give rise to state B. The maximum amplitude of the current block of dA_3 events falls short of the amplitude of the exit spike, suggesting that during the existence of the duplex either the three nucleotides produce spikes that are so short-lived they are filtered at 10 kHz, or that full penetration of the barrel does not occur. We favor the latter interpretation because of the relatively large amplitude of the exit spike, which can be taken to be characteristic of penetration of the barrel. However, the form of the exit spike is not a completely reliable argument against state B for dA_3-oligo-B, because the transient spikes may be shorter than the exit spikes, reflecting their slightly different molecular nature. Only the exit spikes include the separation of the duplex and the complete passage of an oligonucleotide to the *trans* side of the pore.

The data indicate that dA_4-oligo-B and longer oligonucleotides are capable of penetrating the inner constriction,

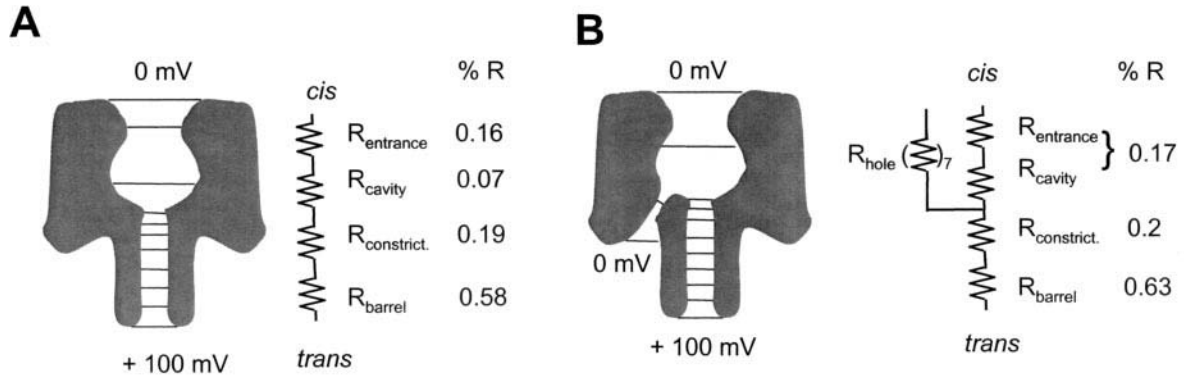

FIGURE 6 Calculated lines of equipotential within the αHL pore. The values are estimated for ψ_M + 100 mV; the local potential $\psi_S(d)$ is ignored (see the text). (*A*) The fractional resistance of four segments of the pore were estimated based on $R \propto l/d^2$, where l is the length of the segment and d is the diameter. The following values were used (l, d in Å): entrance 19, 25; cavity 28, 45; constriction 8, 15; barrel 45, 20. (*B*) The fractional resistance of segments of the pore incorporating the "side exits" in the cap of the pore. The dimensions of the side exits were taken to be l = 15 Å, d = 5 Å).

which is in keeping with the known dimensions of the pore (Song et al., 1996). The shorter dA_2-oligo-B approaches the constriction, as evidenced by increased current noise while the duplex is present. The length of dA_2-oligo-B including the linker is ~42 Å, as estimated by using previous determinations of the dimensions of nucleic acids ((Saenger, 1983), the duplex was assumed to be a double helix) and the expected bond lengths and angles for the linker. It should be noted that this approach yields an actual measurement of "d" and not the electrical distance "δ," which is the outcome of several other approaches. The C_α-C_α distance between residue 17, the point of attachment of oligo-A, and residue 111, in the constriction, is 45 Å, while a surface-to-surface measurement between these sites yields ~43 Å.

When another series of oligonucleotides, dT_N-oligo-B, was hybridized to $H_6$17C-oligo-A_1, the binding events were similar to those observed with dA_N-oligo-B (Fig. 3). Similarly, additional noise was first perceptible with the dT_2-oligo-B. Transitions between states A and B were apparent with dT_4-oligo-B, and two states were approximately equally populated for dT_7-oligo-B. For dA_N-oligo-B the states are equally populated for dA_5-oligo-B. It is possible that this difference is related to the lower propensity of oligo-dT to form secondary structure and the greater flexibility of oligo-dT chains (Bonnet et al., 1998; Meller et al., 2000; Bar-Ziv and Libchaber, 2001), which might make them less likely to thread through the inner constriction.

The lifetimes of the type 2 binding events are dependent on the length of the 5′-extension (Fig. 4). The findings are consistent with a model in which the voltage-dependent step is a preequilibrium between states A and B, and in which dissociation from state B is faster than dissociation from state A. We have no ready explanation for the decrease in the dissociation rate for dA_1-oligo-B compared to oligo-B itself. The increased rate of dissociation in state B might arise from the fact that the oligonucleotide is already threaded into the β-barrel (the exit route) or because of a voltage dependence of k_{off}. The latter is not expected to be large because the movement in the potential gradient to attain the transition state is small, but its existence is supported by measurements of the voltage-dependence of the lifetime of dA_8-oligo-B and dT_9-oligo-B type 2 binding events (Fig. 5 *B*). At ≥+100 mV, both bound dA_8-oligo-B and dT_9-oligo-B are predominantly in state B. Therefore, assuming that simple transition state theory applies, the lifetime of this state should exhibit an exponential dependence on applied potential (Moczydlowski, 1986). While that is not the case, the negative slope of ln τ versus ΔV (Fig. 5 *B*) suggests that the oligonucleotides "feel" the transmembrane potential. By contrast, in the case of oligo B, which does not reach into the transmembrane β-barrel, the slope is weakly positive (Fig. 5 *C*).

Whatever the detailed mechanism of dissociation might be, the results suggest that the duplexed oligonucleotide does not sense a strong field in the cavity in the range of applied potentials we have examined. This fact has proved useful in measurements of the kinetics and thermodynamics of duplex formation, in which the results were comparable with those determined in solution (Howorka et al., 2001b). The weak strength of the field ($d\psi/dd$) in the cavity is reasonable on geometric and structural grounds (Fig. 6). The cavity is the widest part of the lumen and is expected to be of low resistance (Fig. 6 *A*). Furthermore, the cavity appears to contain holes that connect the lumen to the aqueous phase on the *cis* side of the bilayer (Fig. 6 *B*). In either case, the voltage drop in the cavity is expected to be <10 mV in an applied potential of +100 mV, while the drop across the constriction is ~20 mV followed by a drop of ~1.3 mV $Å^{-1}$ in the barrel. This simple description is complicated by the fact that the potential profile will change during duplex formation, as implied by the large drop in conductance. Finally, the contributions of the local electrostatic potential, ψ_S, are likely to be small given the high salt concentration (2 M KCl) used in our experiments and the

wide cross-section of the cavity, and this was supported by calculations using the software package Spock (Christopher, 1998) (data not shown). This situation contrasts with the case of narrow ion channels, such as the acetylcholine receptor, at lower salt concentrations, where the magnitude of ψ_M and ψ_S can be comparable (Adcock et al., 1998; Pascual and Karlin, 1998; Wilson et al., 2000).

In summary, the method we have proposed is a convenient way to probe distance and potential within a channel or pore. Only one engineered construct need be made and the subsequent experiments can be executed with a series of synthetic oligonucleotides. However, the duplex that is formed takes up a large space and the procedure would not be expected to work in narrow channels and cannot be used for measuring short distances. This problem might be circumvented by the direct attachment of different probes, although this requires additional work (Blaustein et al., 2000). A second problem is that formation of a DNA duplex must alter the potential profile across the pore. Finally, because the dissociation step for a duplex is not expected to be highly voltage-dependent, we cannot determine the magnitude of the potential drop in the cavity. Nevertheless, the increase in the duplex lifetime for dA_1-oligo-B and dT_1-oligo-B in the presence of a strong positive applied potential suggests that the drop is small, in agreement with structural considerations (Fig. 6).

We thank Orit Braha for her advice, and Katerina Kouri and Rosa Lemmens-Gruber for their assistance with reacquiring data.

This work was supported by the U.S. Department of Energy, the National Institutes of Health, the Office of Naval Research (Multidisciplinary University Research Initiative 1999), and the Texas Advanced Technology Program. S.H. held fellowships from the Austrian Science Foundation (Fonds zur Förderung der wissenschaftlichen Forschung) and the Max-Kade Foundation.

REFERENCES

Adcock, C., G. R. Smith, and M. S. P. Sansom. 1998. Electrostatics and the ion selectivity of ligand-gated channels. *Biophys. J.* 75:1211–1222.

Bar-Ziv, R., and A. Libchaber. 2001. Effects of DNA sequence and structure on binding of RecA to single-stranded DNA. *Proc. Natl. Acad. Sci. U.S.A.* 98:9068–9073.

Blaustein, R. O., P. A. Cole, C. Williams, and C. Miller. 2000. Tethered blockers as molecular "tape measures" for a voltage-gated K^+ channel. *Nat. Struct. Biol.* 7:309–311.

Bonnet, G., O. Krichevsky, and A. Libchaber. 1998. Kinetics of conformational fluctuations in DNA hairpin-loops. *Proc. Natl. Acad. Sci. U.S.A.* 95:8602–8606.

Braha, O., B. Walker, S. Cheley, J. J. Kasianowicz, L. Song, J. E. Gouaux, and H. Bayley. 1997. Designed protein pores as components for biosensors. *Chem. Biol.* 4:497–505.

Cheley, S., O. Braha, X. Lu, S. Conlan, and H. Bayley. 1999. A functional protein pore with a "retro" transmembrane domain. *Protein Sci.* 8:1257–1267.

Cheung, M., and M. H. Akabas. 1997. Locating the anion-selectivity filter of the cystic fibrosis transmembrane conductance regulator (CFTR) chloride channel. *J. Gen. Physiol.* 109:289–299.

Chiamvimonvat, N., M. T. Pérez-Garcia, R. Ranjan, E. Marban, and G. F. Tomaselli. 1996. Depth asymmetries of the pore-lining segments of the Na+ channel revealed by cysteine mutagenesis. *Neuron.* 16:1037–1047.

Chory, J., and J. D. Pollard. 1999. Resolution and recovery of small DNA fragments. *In* Current Protocols in Molecular Biology. F. M. Ausubel, R. Brent, R. E. Kingston, D. D. Moore, J. G. Seidman, J. A. Smith, and K. Struhl, editors. John Wiley and Sons, Inc., New York. 2:7.1–2.7.8.

Christopher, J. A. 1998. SPOCK: the structural properties observation and calculation kit (program manual). Center for Macromolecular Design, Texas A&M University, College Station, TX.

Corey, D. R., D. Munoz-Medellin, and A. Huang. 1995. Strand invasion by oligonucleotide-nuclease conjugates. *Bioconjugate Chem.* 6:93–100.

Corringer, P. J., S. Bertrand, J. L. Galzi, A. Devillers-Thiery, J. P. Changeux, and D. Bertrand. 1999. Mutational analysis of the charge selectivity filter of the alpha7 nicotinic acid receptor. *Neuron.* 22:831–843.

Hanke, W., and W.-R. Schlue. 1993. Planar Lipid Bilayers. Academic Press, London.

Hille, B. 2001. Ion Channels of Excitable Membranes. Sinauer, Sunderland, MA.

Howorka, S., S. Cheley, and H. Bayley. 2001a. Sequence-specific detection of individual DNA strands using engineered nanopores. *Nat. Biotechnol.* 19:636–639.

Howorka, S., L. Movileanu, O. Braha, and H. Bayley. 2001b. Kinetics of duplex formation for individual DNA strands within a single protein nanopore. *Proc. Natl. Acad. Sci. U.S.A.* 98:12996–13001.

Howorka, S., L. Movileanu, X. Lu, M. Magnon, S. Cheley, O. Braha, and H. Bayley. 2000. A protein pore with a single polymer chain tethered within the lumen. *J. Am. Chem. Soc.* 122:2411–2416.

Imoto, K., C. Busch, B. Sakmann, M. Mishina, T. Konno, J. Nakai, H. Bujo, Y. Mori, K. Fukuda, and S. Numa. 1988. Rings of negatively charged amino acids determine the acetylcholine receptor channel conductance. *Nature.* 335:645–648.

Meller, A., L. Nivon, E. Brandin, J. Golovchenko, and D. Branton. 2000. Rapid nanopore discrimination between single polynucleotide molecules. *Proc. Natl. Acad. Sci. U.S.A.* 97:1079–1084.

Moczydlowski, E. 1986. Single-channel enzymology. In Ion Channel Reconstitution. C. Miller, editor. Plenum Press, New York. 75–113.

Montal, M., and P. Mueller. 1972. Formation of bimolecular membranes from lipid monolayers and study of their electrical properties. *Proc. Natl. Acad. Sci. U.S.A.* 69:3561–3566.

Movileanu, L., S. Howorka, O. Braha, and H. Bayley. 2000. Detecting protein analytes that modulate transmembrane movement of a polymer chain within a single protein pore. *Nat. Biotechnol.* 18:1091–1095.

Pascual, J. M., and A. Karlin. 1998. State-dependent accessibility and electrostatic potential in the channel of the acetylcholine receptor: inferences from the rates of reaction of thiosulfonates with substituted cysteines in the M2 segment of the alpha subunit. *J. Gen. Physiol.* 111:717–739.

Roux, B., and R. MacKinnon. 1999. The cavity and pore helices in the KcsA K^+ channel: electrostatic stabilization of monovalent cations. *Science.* 285:100–102.

Saenger, W. 1983. Principles of Nucleic Acid Structure. Springer Verlag, New York.

Song, L., M. R. Hobaugh, C. Shustak, S. Cheley, H. Bayley, and J. E. Gouaux. 1996. Structure of staphylococcal α-hemolysin, a heptameric transmembrane pore. *Science.* 274:1859–1865.

Stauffer, D. A., and A. Karlin. 1994. The electrostatic potential of the acetylcholine binding sites in the nicotinic receptor probed by reactions of binding-site cysteines with charged methanethiosulfonates. *Biochemistry.* 33:6840–6849.

Vercoutere, W., S. Winters-Hilt, H. Olsen, D. Deamer, D. Haussler, and M. Akeson. 2001. Rapid discrimination among individual DNA hairpin molecules at single-nucleotide resolution using an ion channel. *Nat. Biotechnol.* 19:248–252.

Wilson, G. G., J. M. Pascual, N. Brooijmans, D. Murray, and A. Karlin. 2000. The intrinsic electrostatic potential and the intermediate ring of charge in the acetylcholine receptor channel. *J. Gen. Physiol.* 115: 93–106.